Electronic Supplementary Information

For the Manuscript Entitled

Fluorescent detection of multiple ions by two related chemosensors: Structural elucidations and logic gate applications

Vijay Kumar,‡ Pramod Kumar‡ and Rajeev Gupta*

Department of Chemistry, University of Delhi, Delhi – 110 007

Determination of Stern-Volmer constants (K_{SV}) and detection limits: Stern-Volmer constants (K_{SV}) were calculated by the slope of Stern–Volmer equation (1)[1,2] where, I_0 and I are the emission intensities of chemosensors L1/L2 in the absence and in the presence of different concentration of a quencher (X = Cu^{2+}, Cd^{2+}, S^{2-} ions) respectively.

$$I_0/I = 1 + K_{SV}[X] \quad (1)$$

The detection limits were calculated using equation (2)[3] where, σ is the standard deviation of ten blank measurements and k is the slope of a plot of fluorescence intensity versus analyte ion concentration.

$$\text{Detection limit: } 3\sigma/k \quad (2)$$

Determination of binding constants (K_b):

From fluorescence spectral titration:

The binding constants (K_b) were calculated by the ratio of intercept and slope in the Benesi-Hildebrand equation (3).[4] Where X = analyte (Cu^{2+}, Al^{3+}, Cd^{2+}, S^{2-} ions), I, I_0 and I_{min} are the emission intensities of L1 or L2 at 418 nm in presence of X, in absence of X and minimum fluorescence intensity in presence of X, respectively.

$$1/(I-I_0) = 1/\{K_b(I_0 - I_{min})[X]\} + 1/(I_0 - I_{min}) \quad (3)$$

From UV-Visible spectral titration:

For the detection of Cu^{2+}, Al^{3+}, Cd^{2+} and S^{2-} ions, binding constant (K_b) was also calculated by UV-visible titrations according to the Benesi-Hildebrand equation (4).

$$1/(A-A_o) = 1/\{K_b(A_{max}-A_o)[X]\} + 1/[A_{max}-A_o] \quad (4)$$

Where, A_o is the absorbance of chemosensors L1 or L2 in the absence of analyte X (Cu^{2+}, Al^{3+}, Cd^{2+} and S^{2-} ions), A is the absorbance in the presence of analyte, A_{max} is absorbance in presence of added analyte X (maximum) and K_b is the binding constant which was determined from ratio of intercept and slope of the straight line of the plot of $1/(A-A_o)$ against 1/[X].

X-ray Crystallography: Single crystal diffraction data for **L2**, **[Cu(L1)$_2$]** and **L2-Cd$^{\#}$** were collected at room temperature with an Oxford XCalibur CCD diffractometer equipped with a graphite monochromatic Mo-*K*α radiation (λ = 0.71073 Å).[5] Data reduction was performed with the CrysAllis-PRO.[5] The structure was solved by direct methods using SIR-92 program[6] and refined on F^2 using all data by full matrix least-squares procedures with SHELXL-2014/7[7] incorporated in WINGX 1.8.05 crystallographic collective package.[8] The hydrogen atoms were placed at the calculated positions and included in the last cycles of the refinement. All calculations were done using the WinGX software package.[9] For complex L2-Cd$^{\#}$, all disordered atoms (S1, C19, C20 and O4) of the coordinated DMSO molecule were fixed at two positions by applying part command with site occupancy factors (SOFs) of 0.5 for all the splitted atoms. In addition, disordered DMSO molecule in L2-Cd$^{\#}$ was modeled using SADI and RIGU restraints.[10] Crystallographic data collection and structure solution parameters are summarized in Table S1. This data can be obtained free of charge from The Cambridge Crystallographic Data Center via www.ccdc.cam.uk/data_request/cif.

Table S1. Crystallographic data collection and structure solution parameters for L2 and L2-Cd$^{\#}$.

	L2	**L2-Cd$^{\#}$**
Empirical formula	$C_{18}H_{14}N_2O_3$	$C_{40}H_{38}CdN_4O_8S_2$
Formula weight	306.32	879.27
T (K)	293	298
Cell system	Monoclinic	Monoclinic
Space group	$P2_1/c$	$C2/c$
a (Å)	16.795(2)	16.2629(5)
b (Å)	4.9853(7)	10.0577(3)
c (Å)	18.303(3)	23.5572(6)
α (°)	90	90
β (°)	108.387 (14)	96.692(3)
γ (°)	90	90
V (Å^3)	1454.3(3)	3826.94(19)
Z	4	4
ρ_{calc} (mg/m^3)	1.399	1.515
F (000)	640.0	1800
Goodness-of-fit (GOF) on F^2	1.023	1.290
Final *R* indices [$I > 2\sigma(I)$]	R_1= 0.0697; WR_2= 0.1685	R_1= 0.0777; WR_2= 0.1853
R indices [all data][a]	R_1= 0.1605; WR_2= 0.1292	R_1= 0.0783; WR_2= 0.1855

[a] $R_1 = \Sigma||F_o| - |F_c||/\Sigma|F_o|$; $wR_2 = \{\Sigma[w(|F_o|^2 - |F_c|^2)^2]/\Sigma[wF_{o4}]\}^{1/2}$

References

1 (a) D. Bansal and R. Gupta, *Dalton Trans.*, 2016, **45**, 502; (b) D. Bansal, G. Kumar, G. Hundal and R. Gupta, *Dalton Trans.*, 2014, **43**, 14865; (c) P. Kumar, V. Kumar and R. Gupta, *RSC Adv.*, 2015, **5**, 97874.

2 A. Ganguly, B. K. Paul, S. Ghosh, S. Kar and N. Guchhait, *Analyst*, 2013, **138**, 6532.

3 C. Liang, W. Bu, C. Li, G. Men, M. Deng, Y. Jiangyao, H. Sun and S. Jiang, *Dalton Trans.*, 2015, **42**, 1827.

4 H. A. Benesi and J. H. Hildebrand, *J. Am. Chem. Soc.*, 1949, **71**, 2703.

5 CrysAlisPro, v. 1.171.33.49b, Oxford Diffraction Ltd., 2009.

6 A. Altomare, G. Cascarano, C. Giacovazzo, A. Guagliardi, J. Appl. Crystallogr. 1993, **26**, 343.

7 G. M. Sheldrick, *SHELXL-2014/7*: *Program for the solution of crystal structures*, University of Gottingen, Gottingen, Germany, 2014.

8 G. M. Sheldrick, *Acta Crystallogr.Sect. A: Found. Crystallogr.*, 2008, **64**, 112.

9 L. J. Farrugia, WinGX, v. 1.70, An Integrated System of Windows Programs for the Solution, Refinement and Analysis of Single- Crystal X-ray Diffraction Data, Department of Chemistry, University of Glasgow, 2003.

10 D. Bansal, R. Gupta, *Dalton Trans.*, 2017, **46**, DOI:10.1039/c6dt04858g.

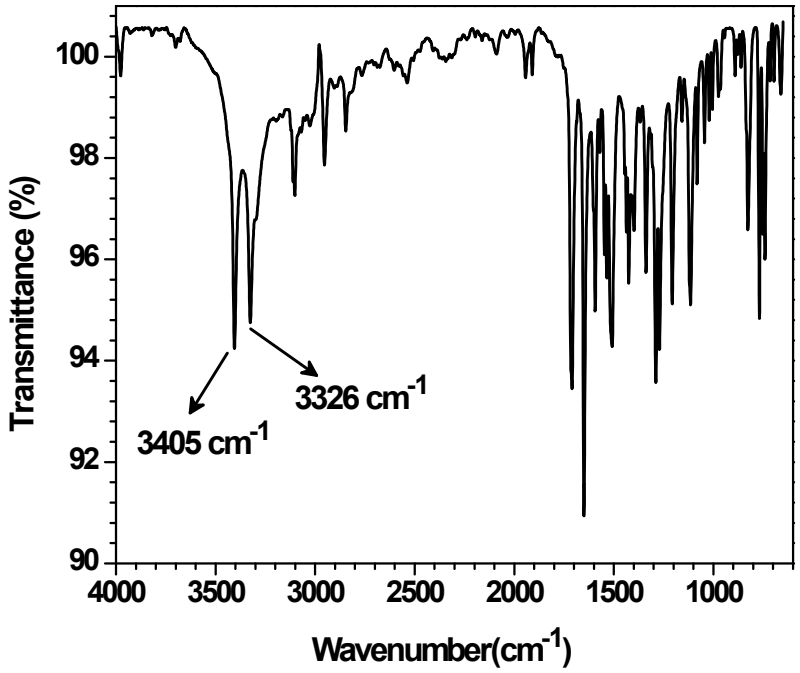

Figure S1. FTIR spectrum of chemosensor L1.

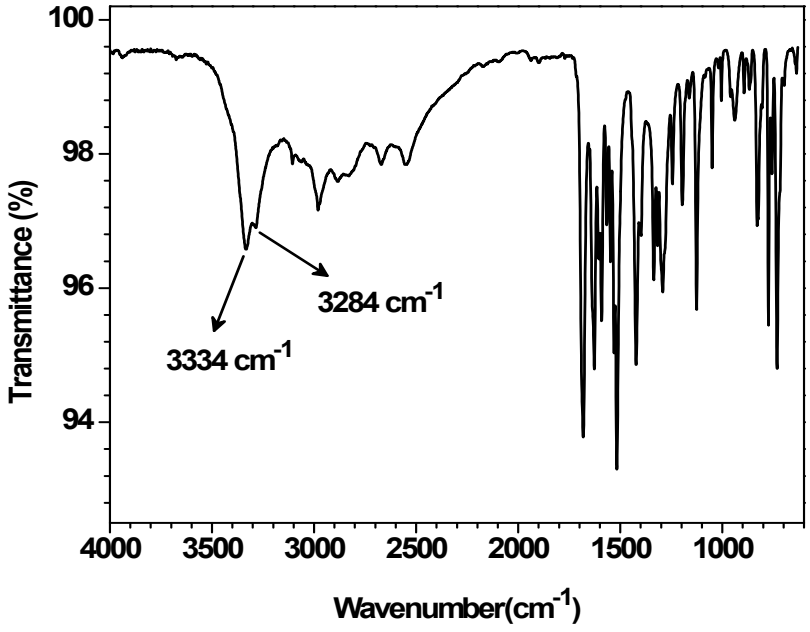

Figure S2. FTIR spectrum of chemosensor L2.

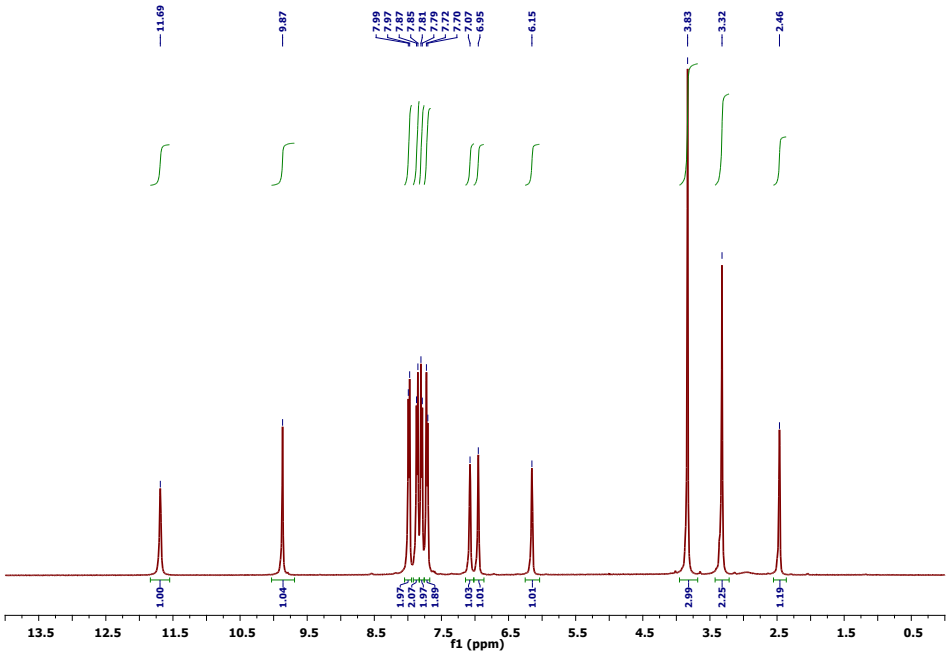

Figure S3. ^{1}H NMR spectrum of chemosensor L1 in DMSO-d_6.

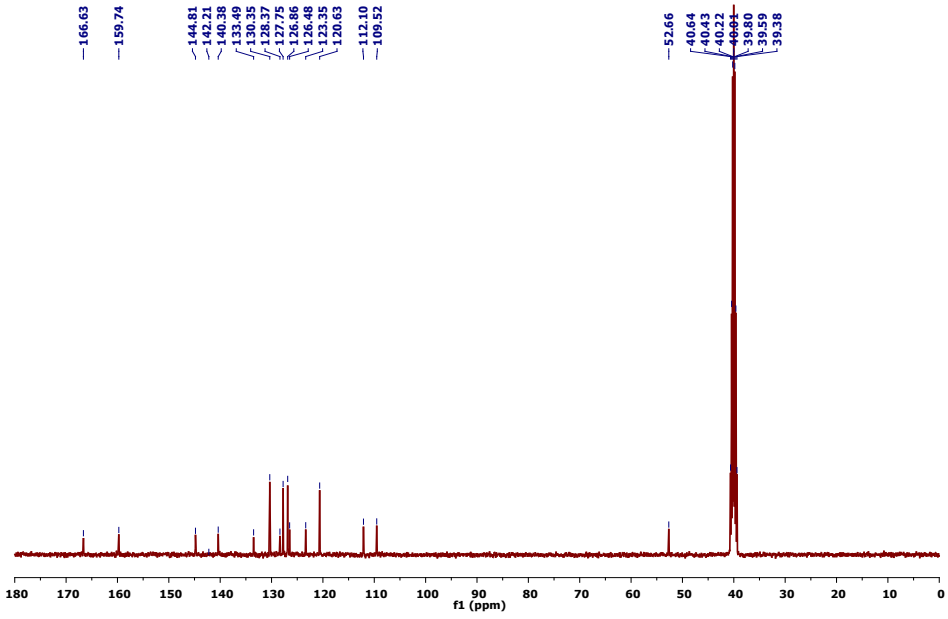

Figure S4. ^{13}C NMR spectrum of chemosensor L1 in DMSO-d_6.

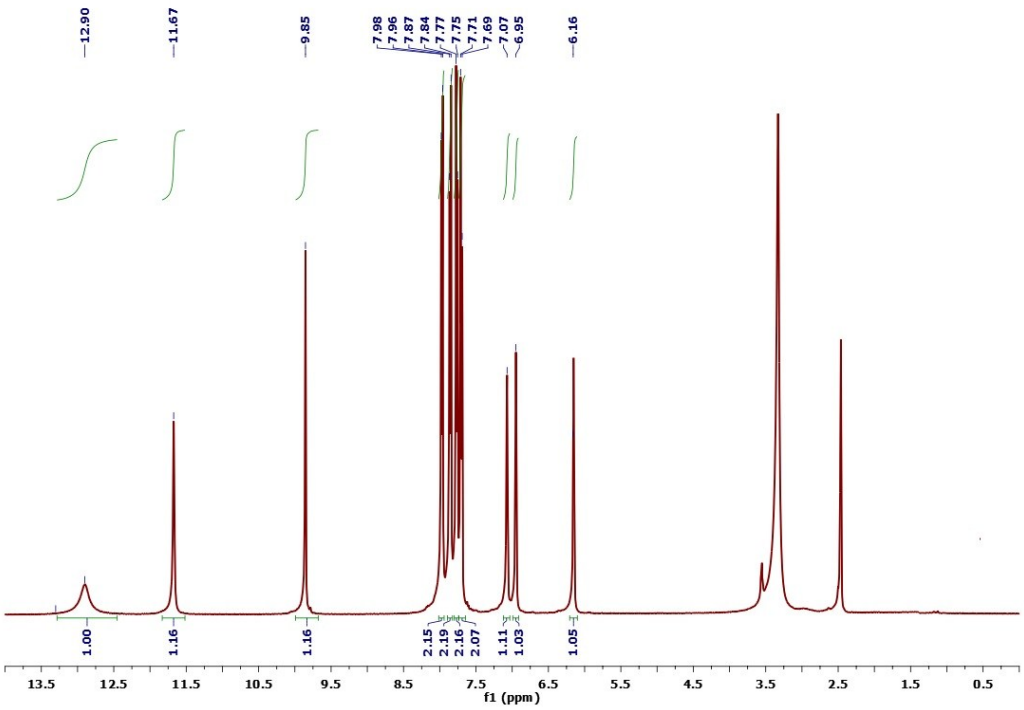

Figure S5. ^{1}H NMR spectrum of chemosensor L2 in DMSO-d_6.

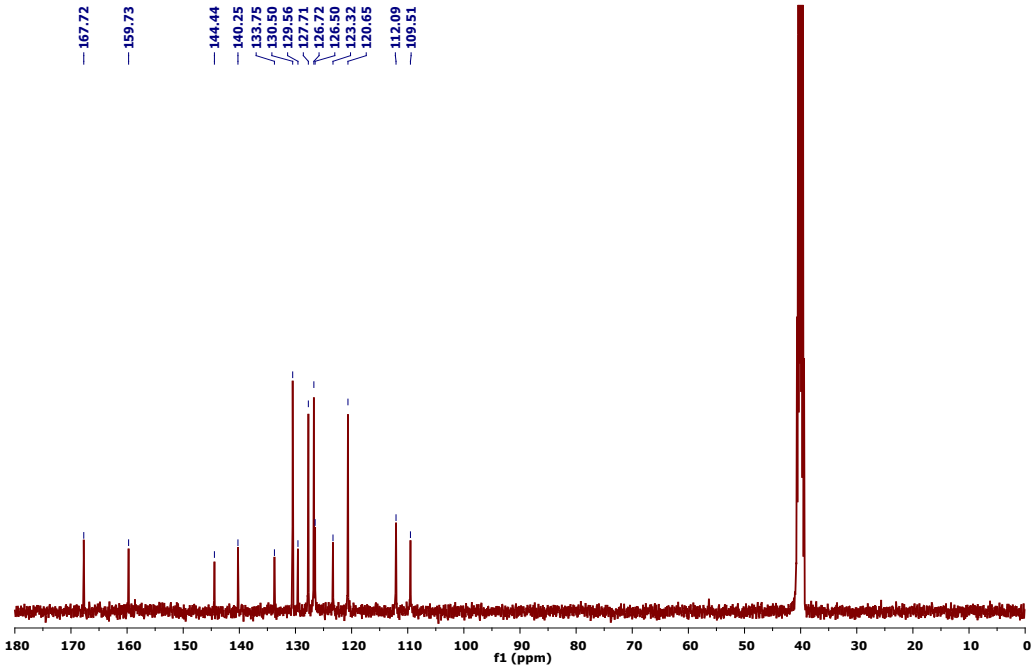

Figure S6. ^{13}C NMR spectrum of chemosensor L2 in DMSO-d_6.

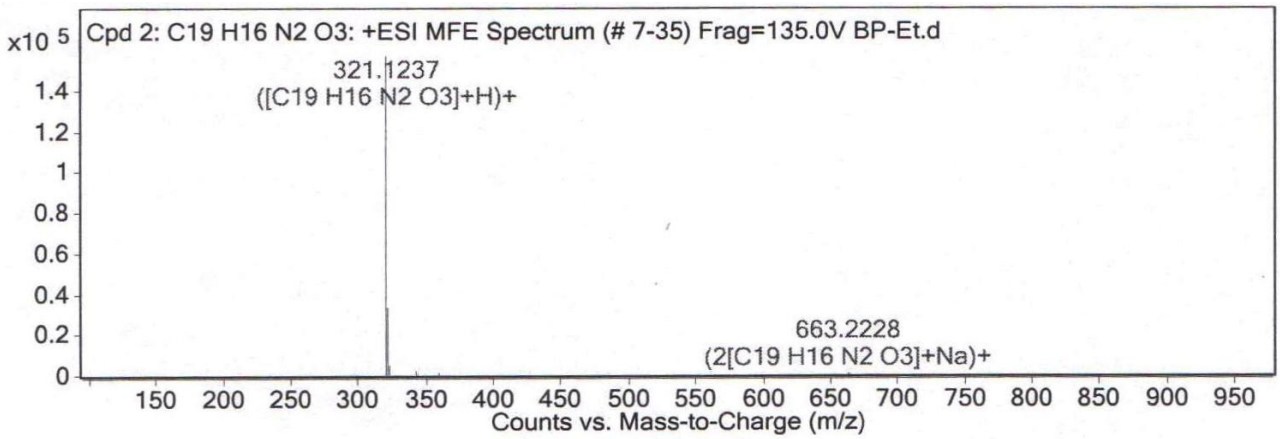

Figure S7. ESI-MS spectrum of chemosensor L1 recorded in methanol.

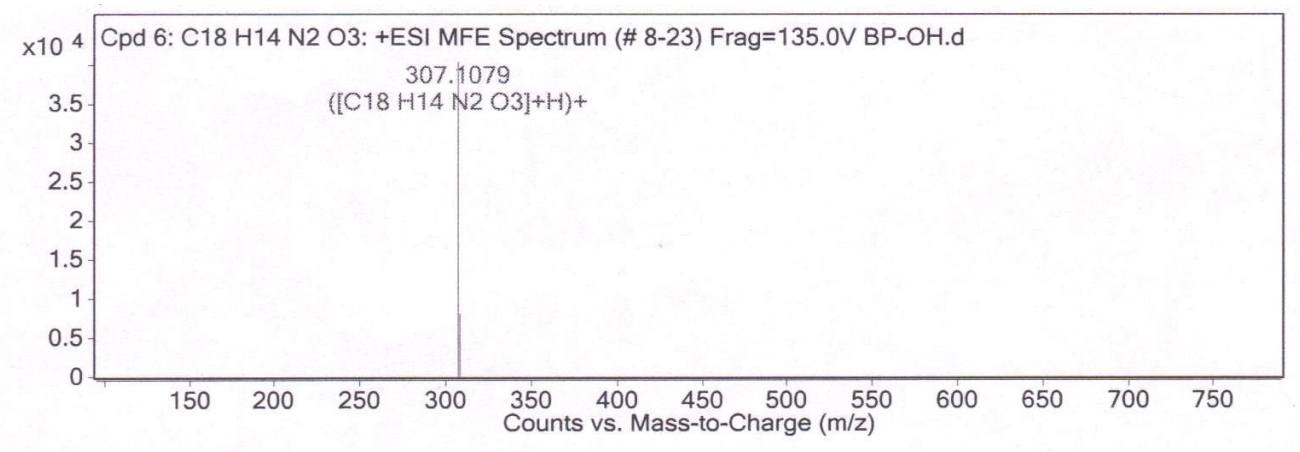

Figure S8. ESI-MS spectrum of chemosensor L2 recorded in methanol.

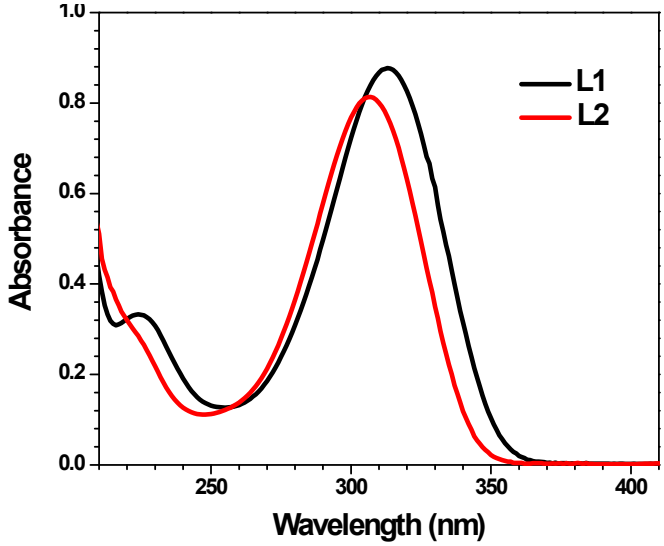

Figure S9. UV-visible spectra of chemosensors L1 (20 μM) and L2 (20 μM) in methanol.

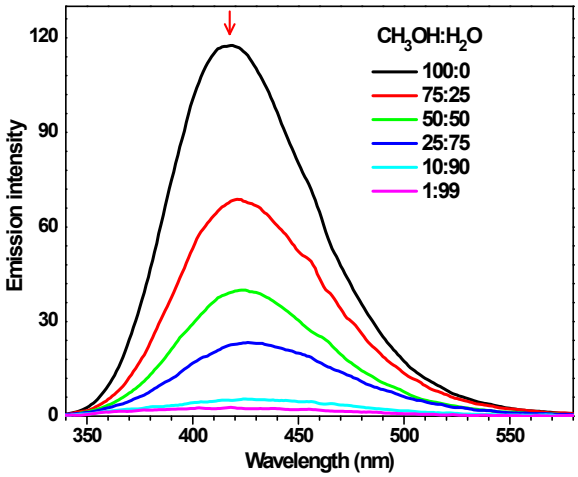

Figure S10. Emission spectra of chemosensor L2 (20 μM) in different proportions of CH_3OH-H_2O mixture (v/v).

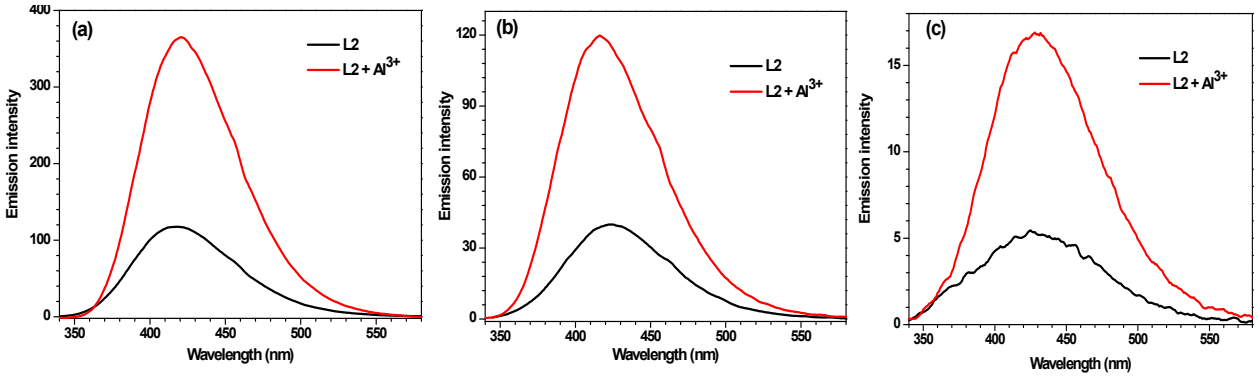

Figure S11. Change in the emission intensity of chemosensor L2 (20 μM) in presence of Al^{3+} ion (100 μM) in (a) CH_3OH/H_2O (100:0), (b) CH_3OH/H_2O (50:50), (c) CH_3OH/H_2O (10:90).

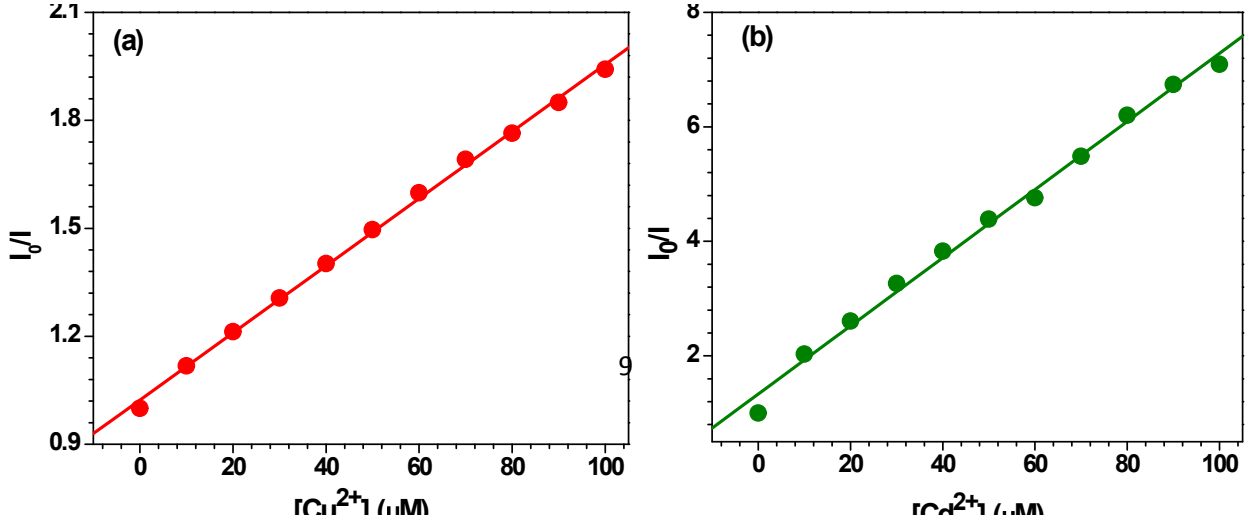

Figure S12. Stern-Volmer plots for the detection of (a) Cu^{2+} ion by chemosensor L1 (20 μM) and (b) Cd^{2+} ion by chemosensor L2 (20 μM).

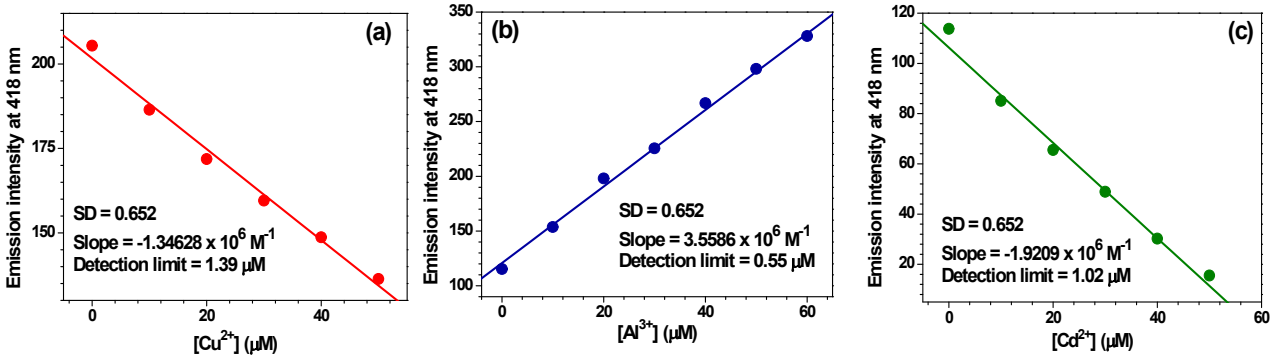

Figure S13. Determination of detection limits for the detection of (a) Cu^{2+} ion by chemosensor L1 (20 μM), (b) Al^{3+} ion by chemosensor L2 (20 μM) and (c) Cd^{2+} ion by chemosensor L2 (20 μM).

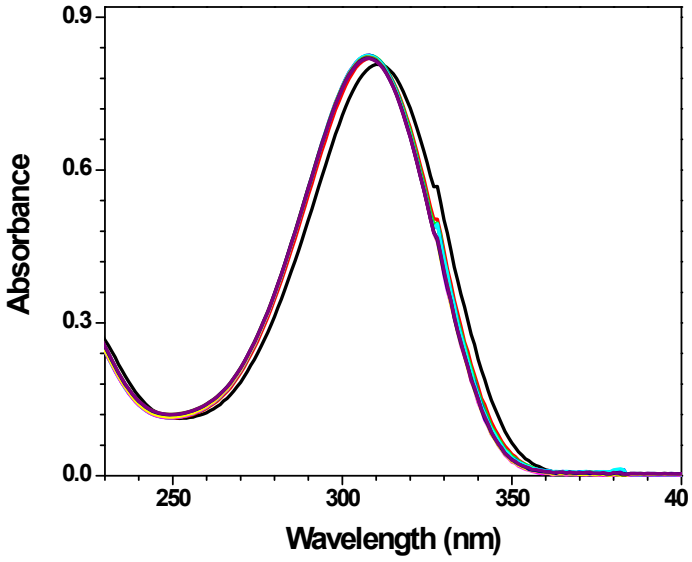

Figure S14. UV-visible spectral titration profile of chemosensor L2 (20 μM) with Cu^{2+} ion (0-100 μM) in methanol.

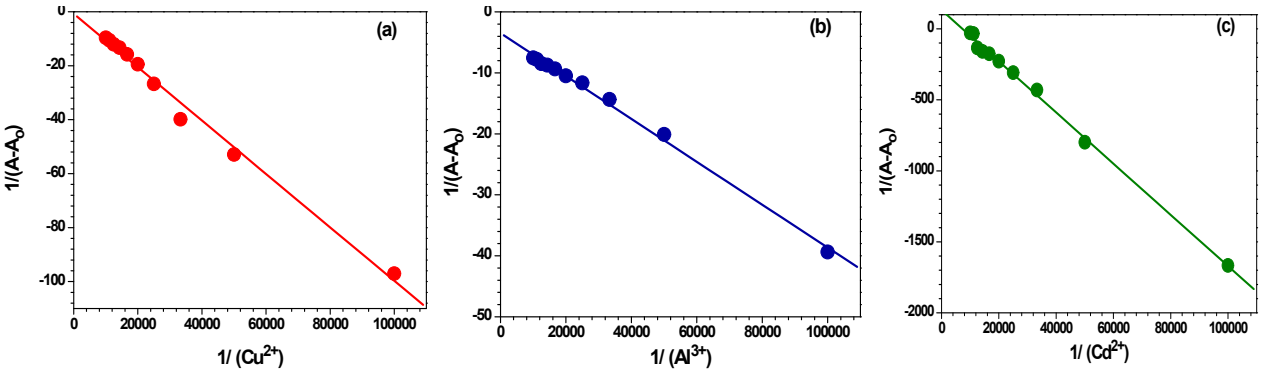

Figure S15. Determination of binding constant (K_b) by UV-visible titrations using the Benesi-Hildbrand plots for the detection of (a) Cu^{2+} ion with L1 (313 nm), (b) Al^{3+} ion with L2 (306 nm) and (c) Cd^{2+} ion with L2 (306 nm).

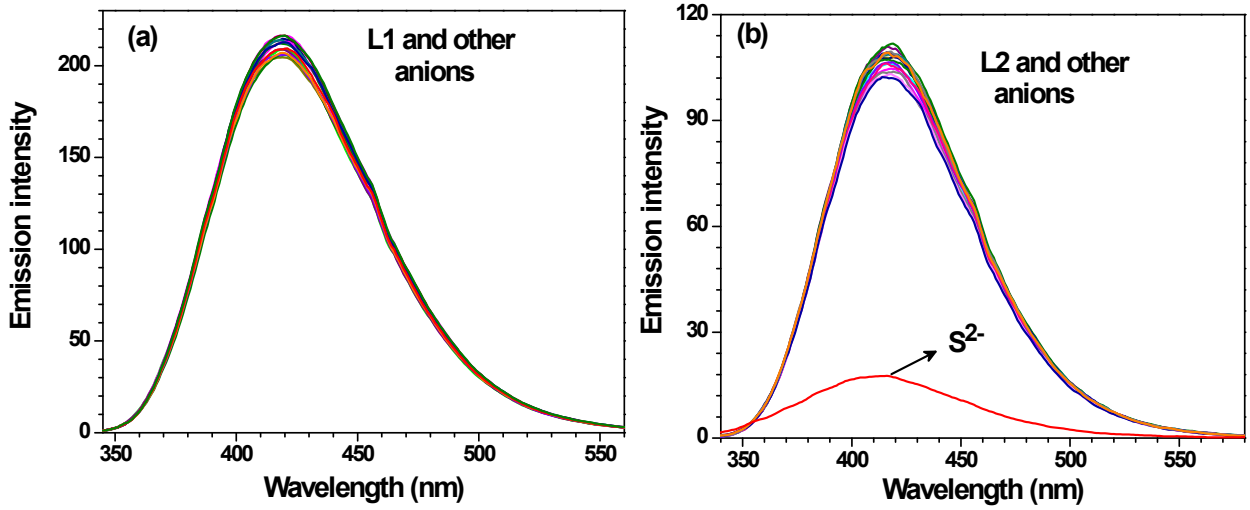

Figure S16. Emission spectra of chemosensors (**a**) L1 (20 μM) and (**b**) L2 (20 μM) in methanol on exposure of 1.2 equivalent of different anions (24 μM).

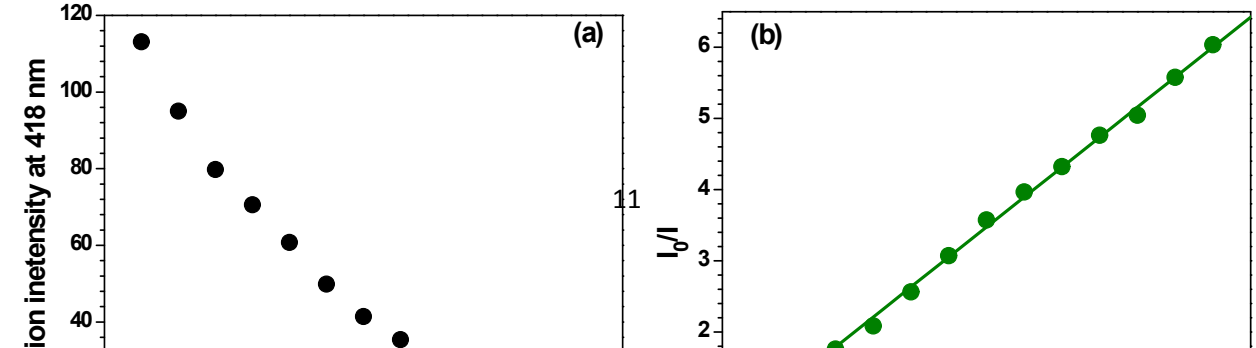

Figure S17. (a) Change in emission intensity of chemosensor L2 (20 μM) at 418 nm with S^{2-} ion (0-24 μM). **(b)** Stern-Volmer plots for chemosensor L2 (20 μM) vs. S^{2-} ion (0-24 μM).

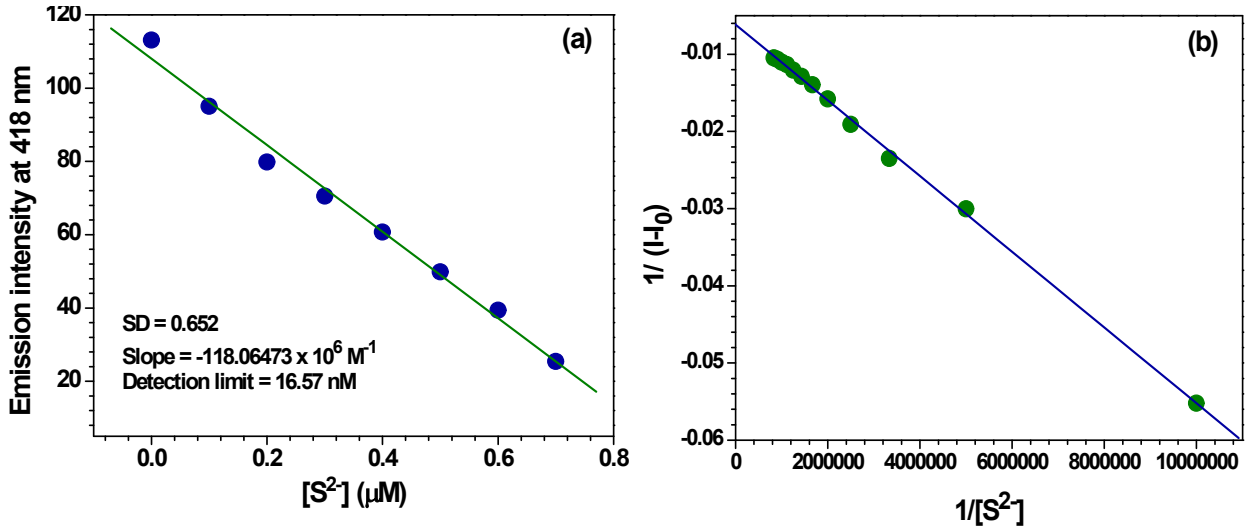

Figure S18. (a) Determination of detection limit of L2 (20 μM) towards S^{2-} ion (0-24 μM). (**b**) Benesi-Hildbrand plot at 418 nm for L2 with S^{2-} ion.

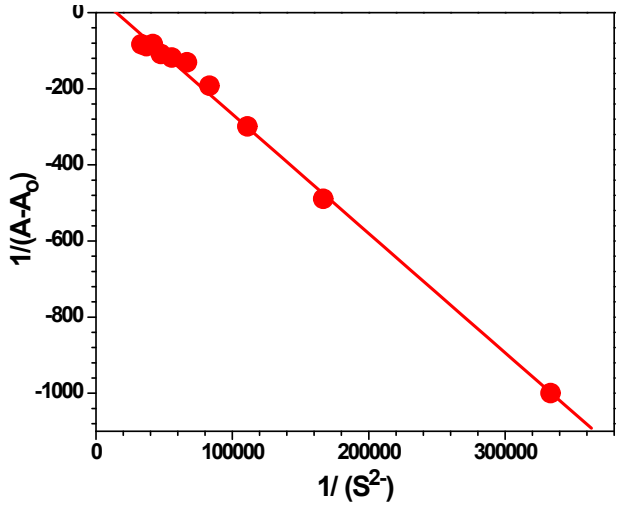

Figure S19. Determination of binding constant (K_b) by UV-visible titration using the Benesi-Hildbrand plot for the detection of S^{2-} ion by chemosensor L2.

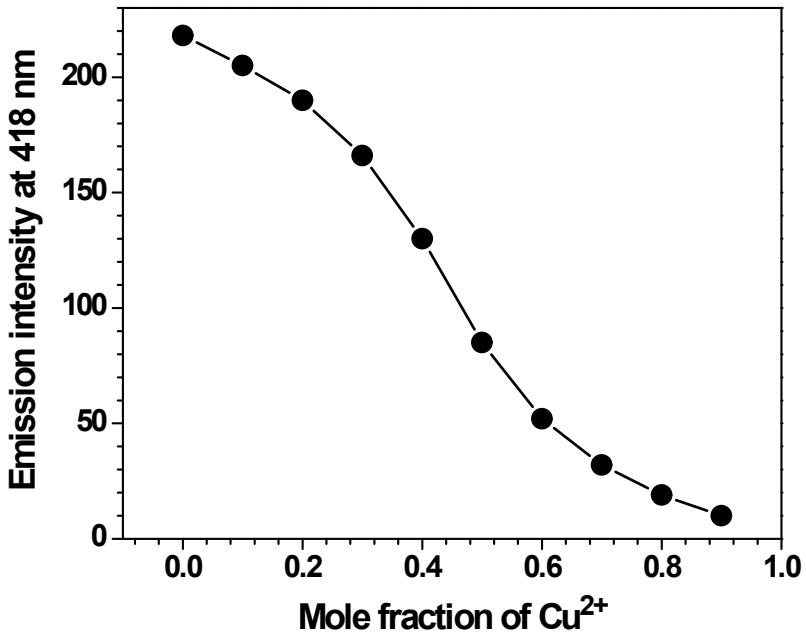

Figure S20. Job's plot for the detection of Cu^{2+} ion by chemosensor L1 in methanol. Total concentrations of Cu^{2+} ion and chemosensor L1 and were maintained at 20 μM.

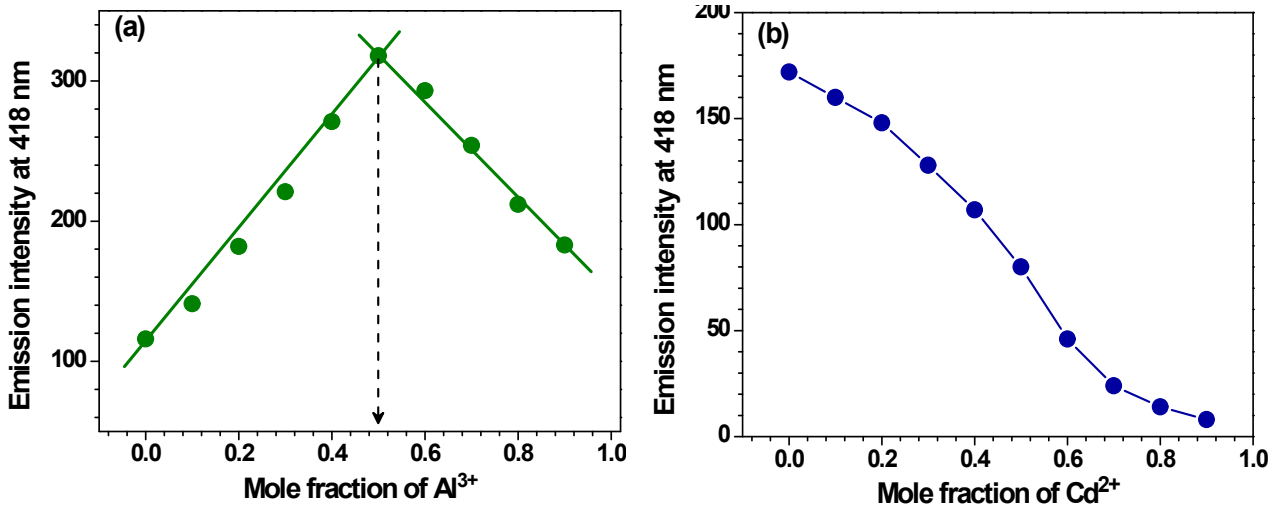

Figure S21. Job's plot for the detection of (a) Al^{3+} ion (b) Cd^{2+} ion by chemosensor L2 in methanol. Total concentrations of Al^{3+}/Cd^{2+} ions and chemosensor L2 were maintained at 50 μM.

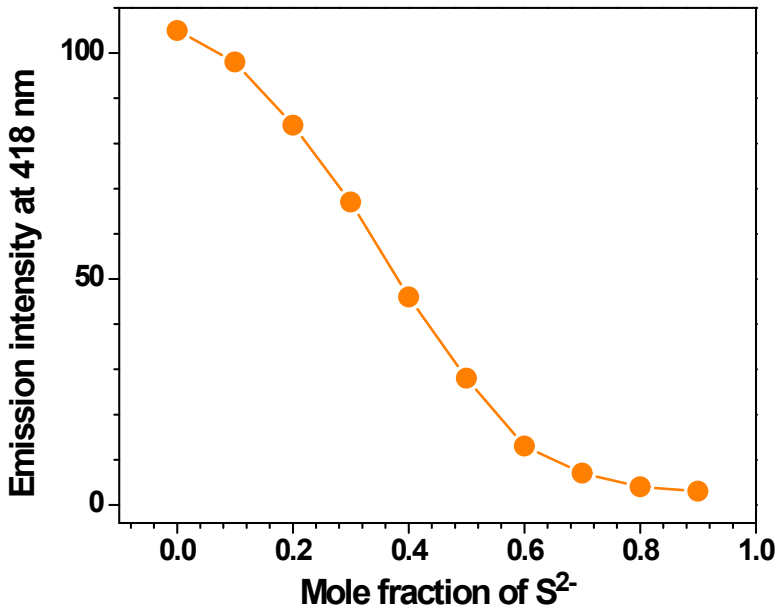

Figure S22. Job's plot for the detection of S^{2-} ion by chemosensor L2 in methanol. Total concentrations of chemosensor L2 and S^{2-} ion were maintained at 20 μM.

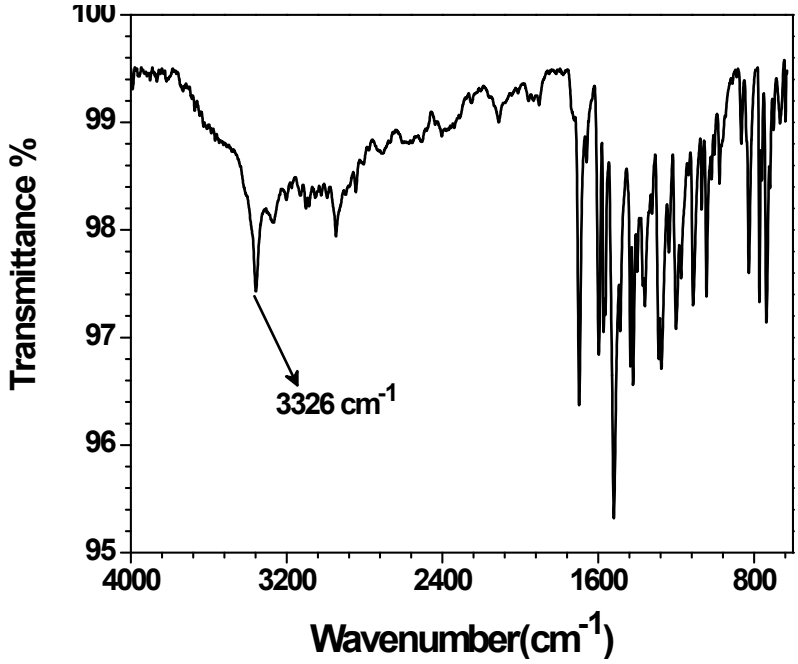

Figure S23. FTIR spectrum of L1-Cu compound.

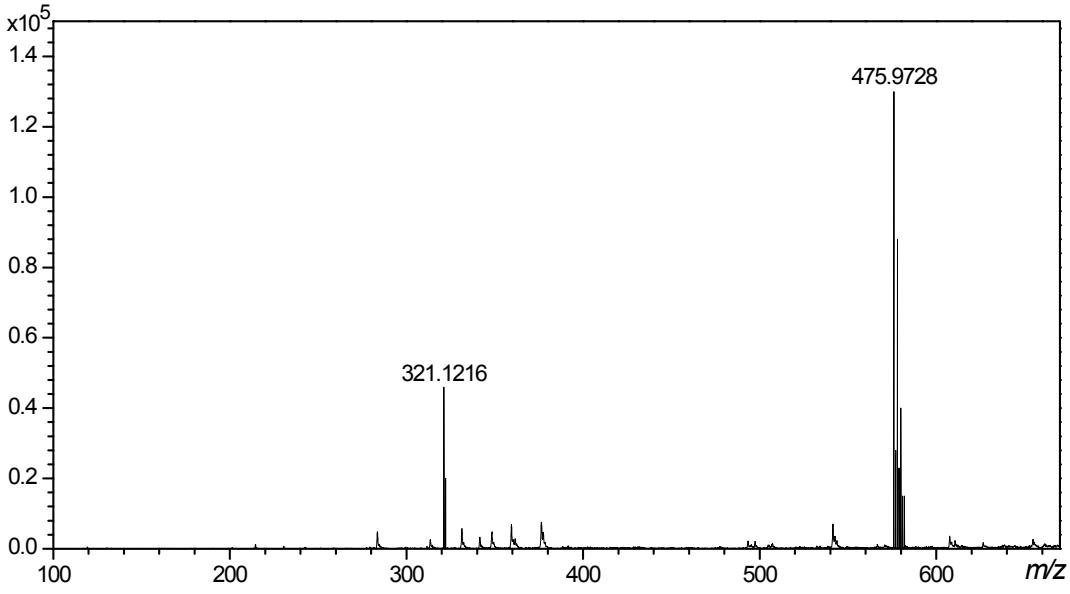

Figure S24. ESI-MS spectrum of L1-Cu recorded in methanol.

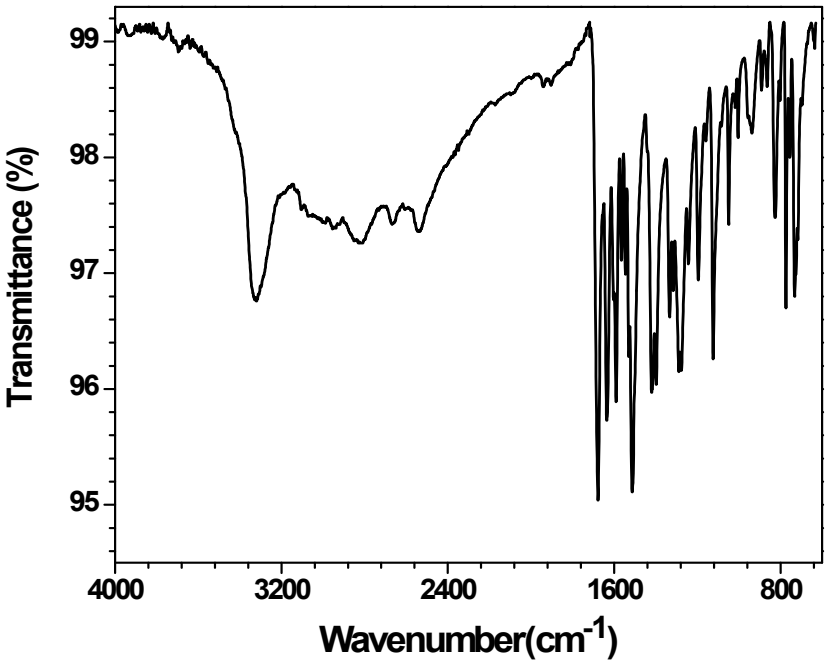

Figure S25. FTIR spectrum of L2-Al compound.

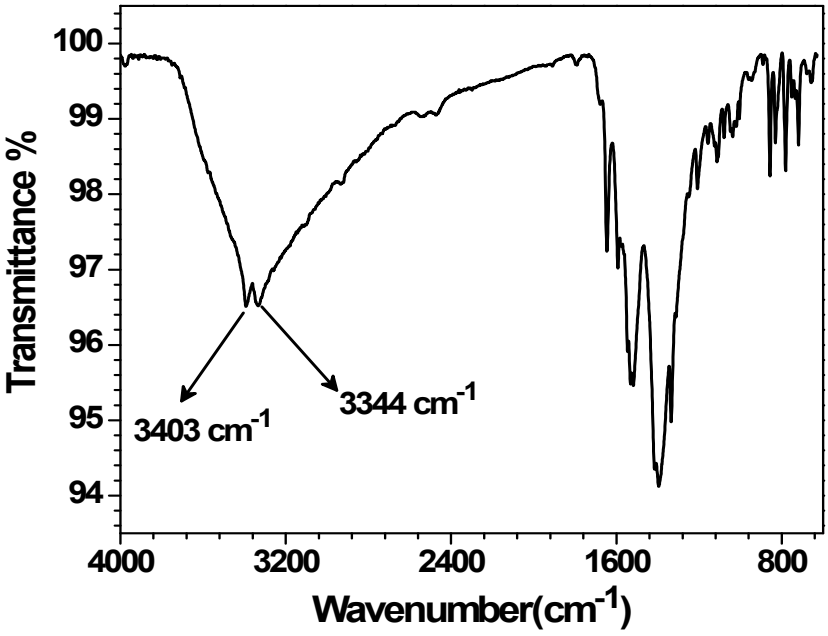

Figure S26. FTIR spectrum of L2-Cd compound.

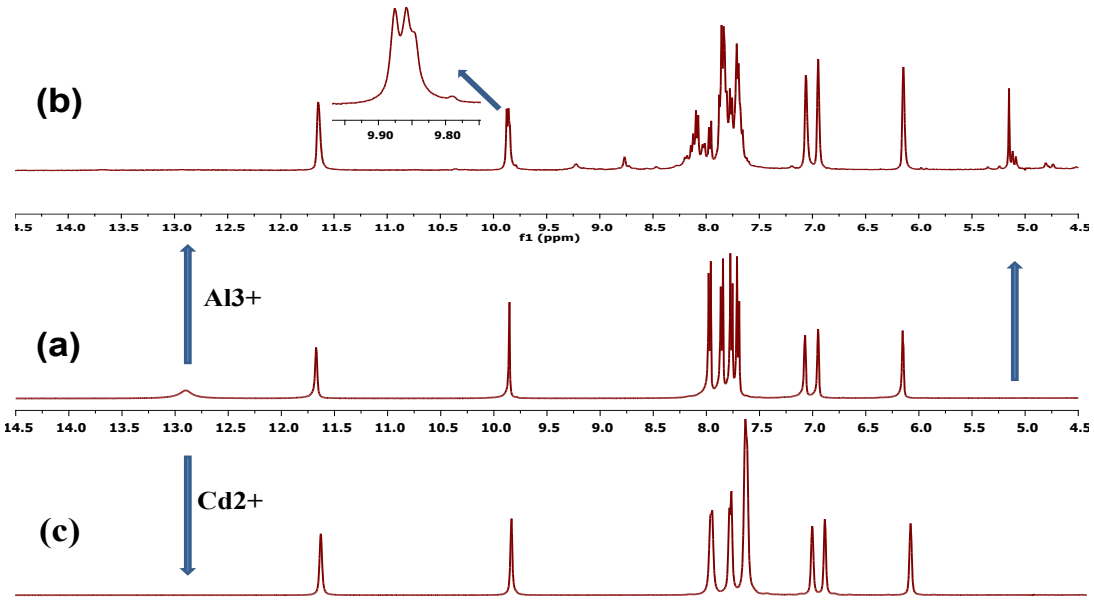

Figure S27. ^{1}H NMR spectra of (**a**) chemosensor L2; (**b**) L2 in presence of $Al(NO_3)_3 \cdot 9H_2O$; (c) L2 in presence of $Cd(CH_3COO)_2$ in DMSO-d_6.

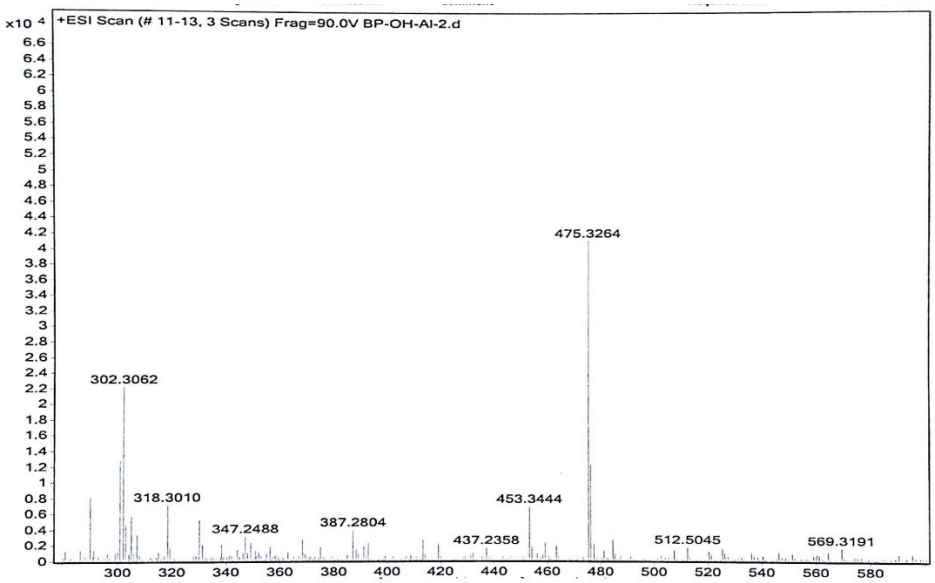

Figure S28. ESI-MS spectrum of L2-Al recorded in methanol.

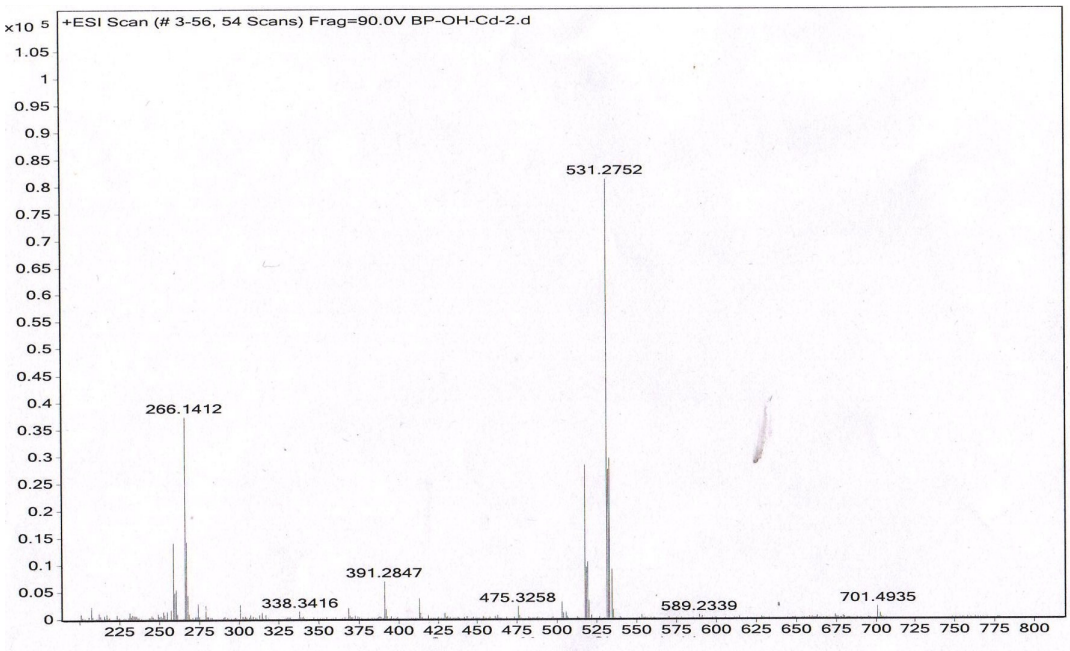

Figure S29. ESI-MS spectrum of L2-Cd recorded in methanol.

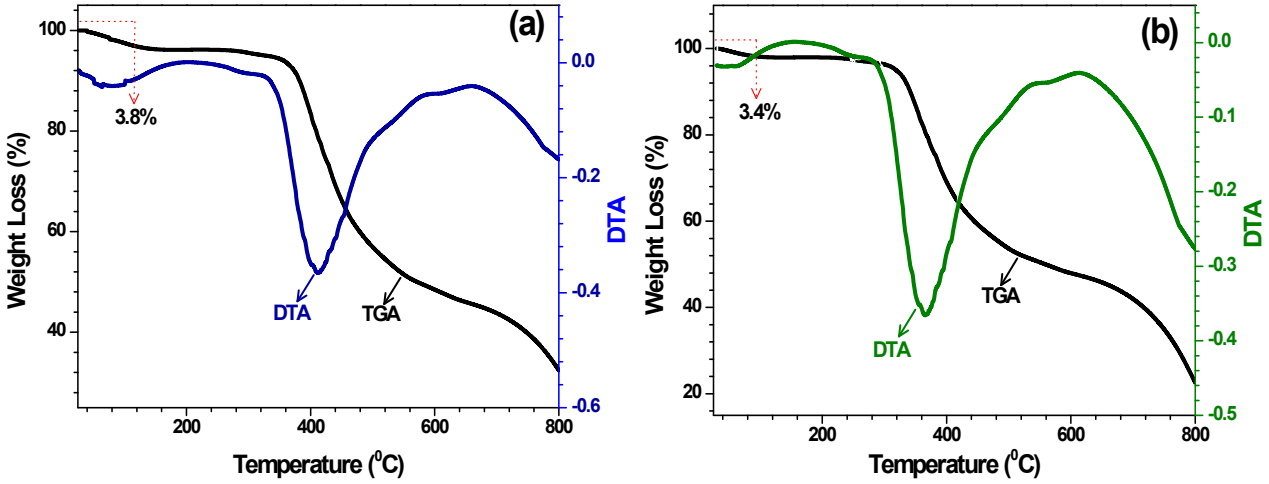

Figure S30. TGA and DTA plots for (a) L2-Al and (b) L2-Cd compounds.

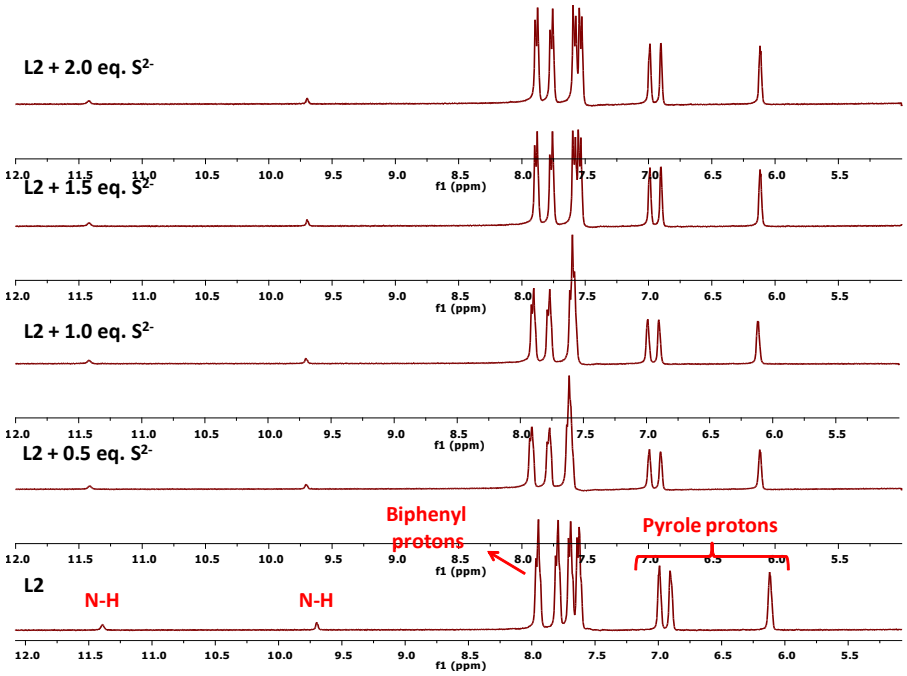

Figure S31. ^{1}H NMR spectra of chemosensor L2 in presence of 0-2.0 equivalent of Na_2S in DMSO-d_6/CD_3OD (50:50 v/v).

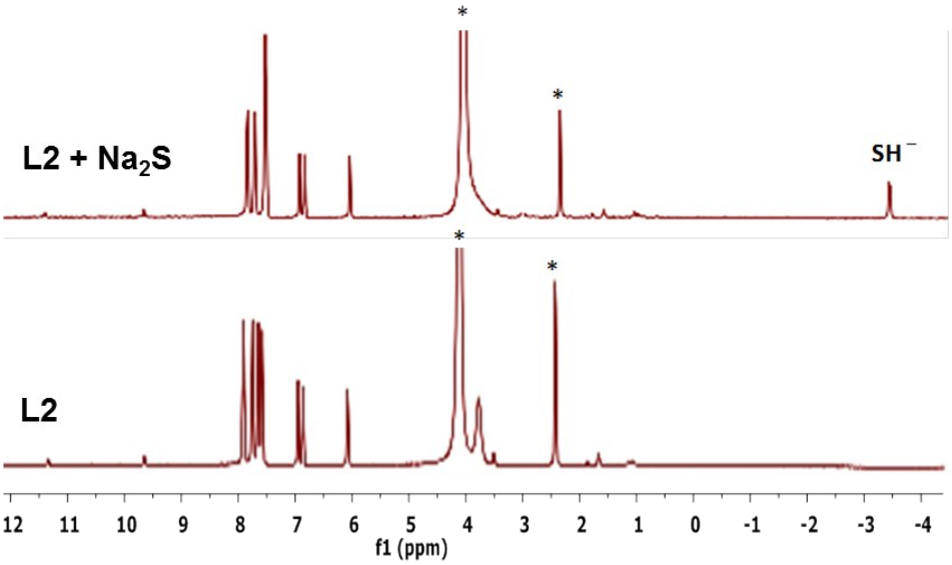

Figure S32. ^{1}H NMR spectra of chemosensor L2 in presence of 2.0 equivalent of Na_2S in DMSO-d_6.

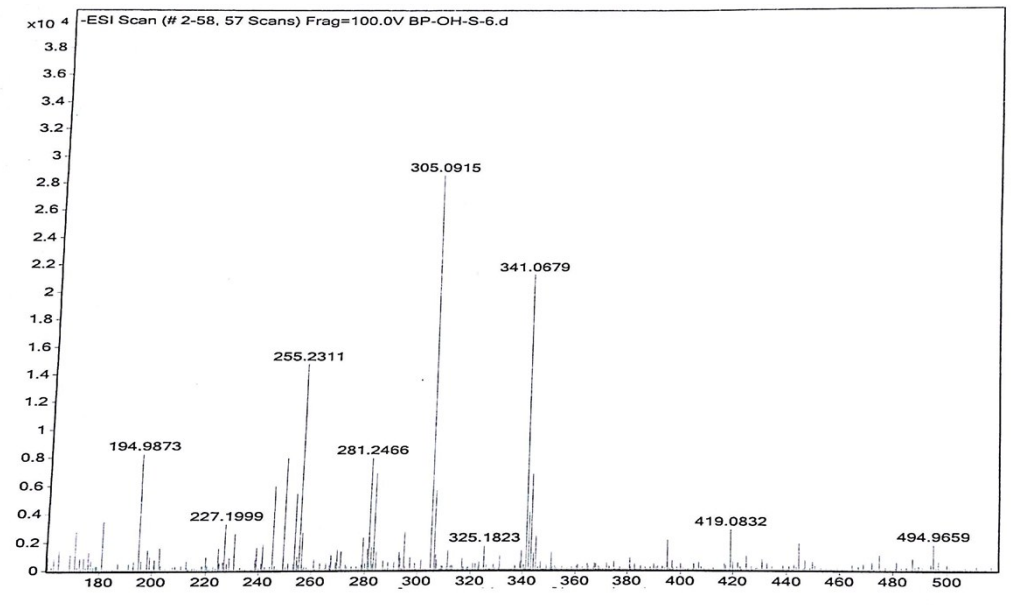

Figure S33. ESI-MS spectrum of L2-S recorded in methanol in negative mode.